Spectrochimica Acta Part A 85 (2012) 31–37

Contents lists available at SciVerse ScienceDirect

Spectrochimica Acta Part A: Molecular and Biomolecular Spectroscopy

journal homepage: www.elsevier.com/locate/saa

Physicochemical and solvatochromic analysis of an imidazole derivative as NLO material

Jayaraman Jayabharathi*, Venugopal Thanikachalam, Marimuthu Venkatesh Perumal

Department of Chemistry, Annamalai University, Annamalainagar 608 002, Tamil Nadu, India

ARTICLE INFO

Article history:
Received 17 June 2011
Received in revised form 17 August 2011
Accepted 24 August 2011

Keywords:
DFT
NLO
NBO
Multi-component linear regression
Octupolar and dipolar components

ABSTRACT

Bioactive imidazole derivative, 2-(2,4-difluorophenyl)-1-phenyl-1H-imidazo[4,5-f][1,10]phenanthroline, has been synthesized and characterized by IR, UV–vis, NMR and elemental (CHN) analysis. The electric dipole moment (μ) and the hyperpolarizability (β) have been studied both experimentally and theoretically, which reveals that the synthesized imidazole derivative possesses non-linear optical (NLO) behavior. This chromophore possess more appropriate ratio of off-diagonal versus diagonal β tensorial component ($r = \beta_{xyy}/\beta_{xxx} = -0.19$) which reflects the in plane nonlinearity anisotropy. Since they have largest $\mu\beta_0$ value, the reported imidazole can be used as potential NLO material. Within this context, reasonable conclusions concerning the steric hindrance in the chromospheres, push–pull character, hyperpolarizability of the imidazole and their application as NLO materials will be drawn. The solvent effect on the absorption and fluorescence bands was analyzed by a multi-component linear regression in which several solvent parameters were analyzed simultaneously.

1. Introduction

Heterocyclic imidazole derivatives have attracted considerable attention because of their unique optical properties [1]. These compounds play very important role in chemistry as mediators for synthetic reactions, primarily for preparing functionalized materials [2]. Imidazole nucleus forms the main structure of human organisms, i.e., the amino acid histidine, Vitamin B_{12}, a component of DNA base structure, purines, histamine and biotin and present in structure of many natural or synthetic drug molecules, i.e., azomycin, cimetidine and metronidazole and also have significant analytical applications due to their fluorescence and chemiluminescence properties [3].

Searching organic materials with non-linear optical (NLO) properties is usually concentrated on molecules with donor–acceptor π-conjugation (D-π-A) and deals with the substituent effects on the degree of π-conjugation, steric hindrance and the hyperpolarizability of the substances. [4]. Nowadays there is an insufficient understanding for designing optimal NLO materials, even certain classes of D-π-A compounds were theoretically studied [5]. Searching for organic materials with NLO properties is usually focused on molecules with donor–acceptor π-conjugation and deals with the systematic investigation of substituent effects on the degree of π-conjugation, steric hindrance and the hyperpolarizability of the molecules. Besides, geometrical arrangement of the molecules in the solid state, their interaction and other physicochemical properties like strong intramolecular charge-transfer absorptions and engineering possibilities are also important [6]. At present, there is an insufficient understanding of all influences for designing optimal NLO materials, even if the influencing factors in certain classes of D-π-A compounds were theoretically studied [7]. To quantify the push-pull effect in D-π-A compounds, bond length alternation (BLA) and out-of-plane distortions of the polarized carbon-carbon double bonds, available from X-ray studies, have been employed for a long time [8]. Alternatively, dipole moment measurements [9], bond lengths [10], barriers to rotation about the partial carbon-carbon double bonds [11] (from dynamic NMR studies), and the occupation quotients (π/π^*) [12] of the bonding (to quantify the acceptor activity) and anti-bonding orbital (to quantify the donor activities) of these carbon-carbon double bonds were adopted. Not only the push–pull effect in D-π-A compounds quantified, but also a linear dependence of the push–pull quotient (π^*/π) on molar hyperpolarizability were detected [10]. Thus, π^*/π is a sensitive parameter of the donor–acceptor quality of compounds for potential NLO applications. The electric dipole moment (μ) and the first-hyperpolarizability (β) revealed that, the synthesized imidazole derivative have non-linear optical (NLO) behavior. This chromophore possesses more appropriate ratio of off-diagonal versus diagonal β tensorial component ($r = \beta_{xyy}/\beta_{xxx}$) which reflects the inplane nonlinearity anisotropy since they have largest $\mu\beta_0$ value, the reported imidazole can be used as potential NLO material and their photophysical properties were investigated in a wide variety of solvents. The solvent effects on the absorption and fluorescence bands were analyzed by a multi-component

* Corresponding author. Tel.: +91 9443940735.
E-mail address: jtchalam2005@yahoo.co.in (J. Jayabharathi).

1386-1425/$ – see front matter © 2011 Elsevier B.V. All rights reserved.
doi:10.1016/j.saa.2011.08.060

linear regression in which several solvent parameters were simultaneously analyzed.

2. Experimental

2.1. Optical measurements and composition analysis

NMR spectra were recorded on a Bruker 400 MHz NMR instrument. The ultraviolet–visible (UV–vis) spectra were measured on a UV–vis spectrophotometer (Perkin Elmer, Lambda 35) and corrected for background due to solvent absorption. Photoluminescence (PL) spectra were recorded on a (Perkin Elmer LS55) fluorescence spectrometer. The infrared spectra were recorded on a Avatar 330-Thermo Nicolet FT-IR spectrometer. Mass spectrum was recorded using Agilant 1100 Mass spectrometer.

2.2. Non-linear Optical measurements

The second harmonic generation efficiency was assessed by Kurtz powder technique [11] at IISc., Bangalore, India. It is a well established tool to evaluate the conversion efficiency of non-linear optical materials. A Q-switched Nd:YAG laser operating at the fundamental wavelength of 1064 nm, generating about 4.1 mJ and pulse width of 8 ns was used for the present experimental study. The input laser beam was passed through an IR reflector and then incident on the powder form of the specimen, which was packed in a glass capillary tube. The output energy was detected by a photodiode detector integrated with oscilloscope assembly.

2.3. Computational details

Quantum mechanical calculations were carried out using Gaussian-03 program [12]. As the first step of our DFT calculation, the geometry taken from the starting structure was optimized.

2.3.1. Hyperpolarizability calculation

The density functional theory has been used to calculate the dipole moment (μ), mean polarizability (α) and the total first static hyperpolarizability (β) [13] for dfppip in terms of x, y, z components and is given by following equations:

$$\mu = (\mu_x^2 + \mu_y^2 + \mu_s^2)^{1/2} \tag{1}$$

$$\alpha = \frac{1}{3}(\alpha_{xx} + \alpha_{yy} + \alpha_{zz}) \tag{2}$$

$$\beta_{tot} = (\beta_x^2 + \beta_y^2 + \beta_z^2)^{1/2} \quad \text{(or)}$$

$$\beta_{tot} = [(\beta_{xxx} + \beta_{xyy} + \beta_{xss})^2 + (\beta_{yyy} + \beta_{yzz} + \beta_{yxx})^2 \tag{3}$$

The β components of Gaussian output are reported in atomic units and therefore the calculated values are converted into e.s.u. units (1 a.u. = 8.3693×10^{-33} e.s.u.).

2.3.2. Natural bond orbital (NBO) analysis

The second order Fock matrix was carried out to evaluate the donor–acceptor interactions in the NBO analysis [14]. For each donor (i) and acceptor (j), the stabilization energy $E(2)$ associated with the delocalization $i \rightarrow j$ is estimated as,

$$E(2) = \Delta E_{ij} = q_i \frac{F(i,j)}{\varepsilon_j - \varepsilon_i} \tag{4}$$

where q_i is the donor orbital occupancy, ε_i and ε_j are diagonal elements and $F(i,j)$ is the off diagonal NBO Fock matrix element. The larger the $E(2)$ value, the more intensive is the interaction between electron donors and electron acceptors.

2.4. Synthesis of 2-(2,4-difluorophenyl)-1-phenyl-1H-imidazo[4,5-f][1,10]phenanthroline

The experimental procedure was used as same as described in our recent papers [15–17]. The imidazole derivative, dfppip was synthesized from an unusual four components assembling of a mixture of 1,10-Phenanthroline-5,6-dione, ammonium acetate, aniline and 2,4-difluorobenzaldehyde in distilled ethanol medium. The reaction was monitored by thin layer chromatography for the completion of the reaction. The reaction mixture was then extracted with dichloromethane and the resultant resinous material was purified by column chromatography using benzene:ethyl acetate (9:1) as the eluent. Yield: 60%. mp. 254 °C, Anal. calcd. for $C_{25}H_{14}F_2N_4$: C, 73.5,; H, 3.46; N, 13.72. Found: C, 72.8; H, 3.23; N, 13.17. ^{1}H NMR (500 MHz, $CDCl_3$): δ 7.01–7.10 (m, 3H) [aldehydic phenyl ring], 7.68–7.73 (m, 3H), 8.27–8.33 (m, 2 *ortho* protons of aniline ring), 8.57 (d, 2H, J = 10.4 Hz), 8.85 (d, 2H, J = 8.0 Hz), 9.18 (d, 2H, J = 4.0 Hz). ^{13}C (100 MHz, $CDCl_3$): δ 105.65, 112.37, 117.88, 122.82, 123.45, 123.65, 128.41, 128.77, 130.83, 131.80, 134.43, 143.42, 144.95, 149.26, 159.44, 159.49, 159.81, 159.94, 162.42, 163.63, 166.17. MS: m/z calcd for $[M+H]^+$ 408.9. IR (cm^{-1}): 3062 ($\upsilon_{=C-H}$), 1614 ($\upsilon_{C=N}$),1112–1062 (polyfluorinated compounds).

3. Results and discussion

To analyze the solvatochromic effects, we have checked several methods [18,19]. Neither the absorption nor the fluorescence wavenumbers linearly correlate with the Lippert parameter $\Delta f(\varepsilon,n^2)$ [20], which consider the solvent polarity/polarizability or with the Reichardt parameter $E_T^N(30)$ [19,21], which takes into account several solvent properties (polarity and H-bond donor capacity) in a common parameter. For these reasons, a multi-parameter correlation analysis is employed in which a physicochemical property is linearly correlated with several solvent parameters by means of Eq. (1):

$$(XYZ) = (XYZ)_0 + C_aA + C_bB + C_cC + \ldots \tag{5}$$

where $(XYZ)_0$ is the physicochemical property in an inert solvent and C_a, C_b, C_c and so forth are the adjusted coefficients that reflect the dependence of the physicochemical property (XYZ) on several solvent properties. Solvent properties that mainly affect the photophysical properties of compounds are polarity, H-bond donor capacity and electron donor ability. Different scales for such parameters can be found in the literature, Taft et al. [22] proposed the π^*, α and β scales, whereas more recently Catalan et al. [23] suggested the SPP^N, SA and SB scales to describe the polarity/polarizability, the acidity and basicity of the solvents, respectively.

Fig. 1 shows the obtained correlation between the absorption and fluorescence wavenumbers calculated by the multi-component linear regression employing the Taft-proposed solvent parameters and the experimental values listed in Table 1. The dominant coefficient affecting the absorption and fluorescence bands of this imidazole derivative (dfppip) is that describing the polarity/polarizability of the solvent, C_{π^*} or C_{SPP}^N having a positive value, corroborating the solvatochromic shifts with the solvent polarity. The coefficient controlling the electron releasing capacity or basicity of the solvent, C_β or C_{SB}, is the lowest coefficient (Table 1), hence, the solvent basicity does not play an important role in absorption and fluorescence displacements. The adjusted coefficient representing the acidity of the solvent, C_α or C_{SA} has a negative value, suggesting that the absorption and fluorescence bands shift to lower energies with the increasing acidity of the solvent. This effect can be interpreted in terms of the stabilization of the resonance structures of the chromophore (Fig. 2). In resonance structure "a" all the nitrogens are having lone pair of electrons and that structure

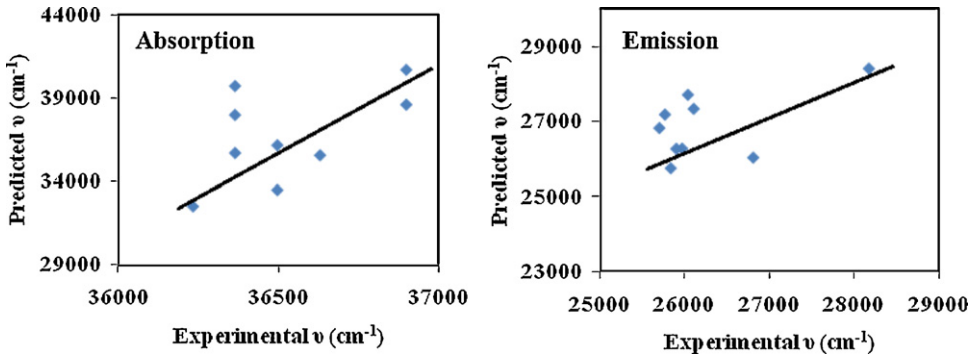

Fig. 1. Correlation between the experimental absorption and fluorescence wavenumber with the predicted values obtained by a multicomponent linear regression using the π^*, α and β-scale (Taft) solvent parameters for dfppip.

Table 1
Adjusted coefficients ($(\upsilon_x)_0$, C_a, C_b and C_c) and correlation coefficients (r) for the multilinear regression analysis of the absorption υ_{ab} and fluorescence υ_{fl} wavenumbers and Stokes shift ($\Delta\upsilon_{ss}$) of the imidazole derivative dfppip with the solvent polarity/polarizability, and the acid and base capacity using the Taft (π^*, α and β) and the Catalan (SPP^N, SA and SB) scales.

(υ_x)	$(\upsilon_x)_0$ cm^{-1}	(π^*)	C_α	C_β	r
λ_{ab}	$(3.63 \pm 0.002) \times 10^4$	$(6.08 \pm 0.574) \times 10^3$	$-(14.81 \pm 1.919) \times 10^3$	$(9.24 \pm 1.541) \times 10^3$	0.97
λ_{fl}	$(2.58 \pm 0.011) \times 10^4$	$(2.16 \pm 2.199) \times 10^3$	$-(10.71 \pm 7.349) \times 10^3$	$(12.838 \pm 5.904) \times 10^3$	0.93
$\Delta\upsilon_{ss} = \upsilon_{ab} - \upsilon_{fl}$	$(1.04 \pm 0.011) \times 10^4$	$(3.91 \pm 2.107) \times 10^3$	$-(4.09 \pm 7.044) \times 10^3$	$-(3.59 \pm 5.658) \times 10^3$	0.95
(υ_x)	$(\upsilon_x)_0$ cm^{-1}	C^N_{SPP}	C_{SA}	C_{SB}	r
λ_{ab}	$(3.66 \pm 0.015) \times 10^4$	$-(3.11 \pm 6.837) \times 10^3$	$(9.86 \pm 42.167) \times 10^3$	$-(8.08 \pm 29.114) \times 10^3$	0.67
λ_{fl}	$(2.58 \pm 0.018) \times 10^4$	$-(0.14 \pm 8.075) \times 10^3$	$(27.82 \pm 37.198) \times 10^3$	$-(43.56 \pm 34.387) \times 10^3$	0.77
$\Delta\upsilon_{ss} = \upsilon_{ab} - \upsilon_{fl}$	$(1.07 \pm 0.024) \times 10^4$	$-(2.97 \pm 10.773) \times 10^3$	$-(17.95 \pm 44.672) \times 10^3$	$(35.48 \pm 45.875) \times 10^3$	0.70

will be stabilized in acidic solvents because this resonance structure is predominant in the S_1 state, and the stabilization of the S_1 state with the solvent acidity would be more important than that of the S_0 state.

3.1. Steric hindrance in imidazoles: X-ray analysis

DFT calculation reveals that the imidazole ring is essentially planar and makes dihedral angle of 91.93° and 88.08° with the phenyl and difluorophenyl rings, respectively. The key twist, designated as α have been examined. α is used to indicate the twist of imidazole ring from the aromatic six-membered ring at C(23), (Fig. 3). The α twist originates from the interaction of substituent at N(15) of the imidazole with the substituent at C(23). The present structural information allows us to further explore the correlation between structural features and fluorescent property. It reveals that α twist is correlated with fluorescent property, the larger the α twist, the more is the drop in the fluorescence quantum yield. Such a clear correlation indicates the importance of coplanarity between imidazole and the aromatic ring at C(23) and this correlation can be ascribed to the conjugation rigidity. When the two adjacent aromatic species are in a coplanar geometry, the p-orbitals from the C–C bond connecting the two species will have maximal overlapping and the two rings will have a rigid and partial delocalized conjugation, as the result, the bond is no longer a pure single bond, as evident from the X-ray data of (dpip). Since X-ray crystal study of the dfppip is currently under progress; its analogous data [24] is taken for comparision. The present bond distance of C23–C24 is 1.475 (4) Å (Table 2) is shorter than the regular single bond distance between two sp2 carbons (1.48 Å) [18], because of delocalization. When the two rings are deviated from each other, the p-orbital overlapping will be reduced. All these XRD data are in good agreement with the theoretical values. However, from the theoretical values it was found that most of the optimized bond lengths, bond angles and dihedral

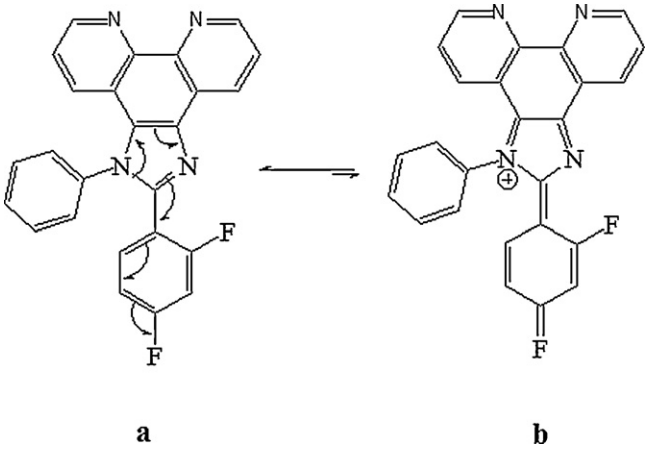

Fig. 2. Resonance structures (a and b) of the imidazole chromophore dfppip.

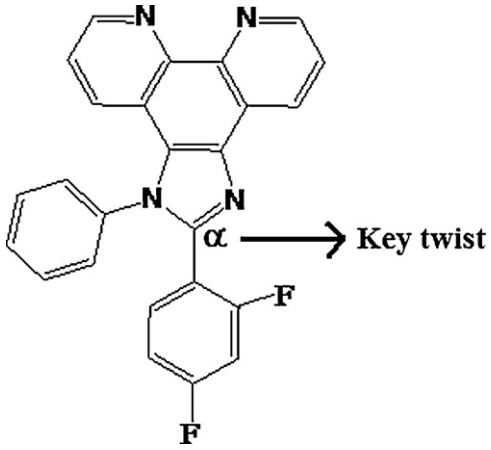

Fig. 3. The key α twist of imidazole ring at C(23).

Table 2
Selected bond lengths, bond angles and torsional angles for the imidazole derivative dfppip.

Bond connectivity	Bond length (Å)[a]	Bond connectivity	Bond angle (°)	Bond connectivity	Torsional angle (°)
N1–C5	1.4106 (1.3840)	N1–C2–N3	111.25707 (112.63)	C4–C5–C6–C7	−179.2650 (−175.39)
N1–C18	1.4361 (1.4402)	N1–C5–C6	132.3278 (131.74)	N1–C5–C6–C7	0.5413 (0.8)
N1–C2	1.4159 (1.3752)	N1–C5–C4	105.0439 (105.14)	N3–C4–C5–C6	179.8021 (176.28)
C2–C24	1.4757 (1.4782)	N1–C18–C19	119.9259 (119.73)	C17–C4–C5–C6	−0.3744 (−3.5)
N3–C4	1.3908 (1.3789)	N1–C18–C23	119.7224 (118.93)	C2–N1–C5–C6	−179.9210 (−175.82)
N3–C2	1.3403 (1.3168)	C2–N1–C5	106.7315 (106.40)	C5–N1–C18–C19	87.8925 (82.65)
C4–C5	1.4190 (1.3770)	C2–C24–C25	122.1452 (121.16)	C5–N1–C18–C23	−93.3349 (−98.62)
C4–C17	1.4475 (1.4330)	C2–C24–C29	119.7692 (119.87)	C5–N1–C2–N3	0.2113 (−0.73)
C5–C6	1.4506 (1.4321)	C2–C3–C4	106.3648 (104.52)	C5–N1–C2–C24	179.5378 (−179.76)
N10–C11	1.3675 (1.3506)	N3–C4–C5	110.0620 (111.31)	C2–N3–C4–C17	−179.6357 (−179.93)
C18–C19	1.4169 (1.3840)	N3–C2–C24	123.5253 (124.59)	C4–N3–C2–C24	179.5785 (179.25)
C18–C23	1.4170 (1.3745)	N3–C4–C17	126.7377 (127.30)	N1–C18–C19–C20	178.3979 (177.39)
C24–C29	1.4322 (1.3860)	C4–C5–C6	122.1671 (123.04)	N1–C18–C23–C22	−178.3995 (−176.22)
C24–C25	1.4153 (1.3890)	C5–C4–C17	122.6599 (121.38)	N1–C2–C24–C29	−91.8453 (−125.55)
C27–F27	1.3203 (0.9500)	C5–N1–C18	128.5619 (128.80)	C18–N1–C2–N3	178.8895 (−174.58)
C29–F29	1.3201 (0.9500)	C24–C25–C26	121.1143 (120.44)	N3–C2–C24–C29	−88.9081 (55.54)
		C24–C29–C28	121.9126 (120.30)	N1–C2–C24–C25	−91.3145 (56.56)
				C2–C24–C29–C28	177.8084 (−177.29)
				C2–N1–C18–C23	88.2840 (73.81)
				C7–C6–C11–N10	0.0443 (0.6)
				C9–N10–C11–C6	0.1303 (−0.1)
				C14–N13–C12–C17	−0.0955 (−3.2)

[a] values given in the brackets are corresponding to XRD values of dpip.

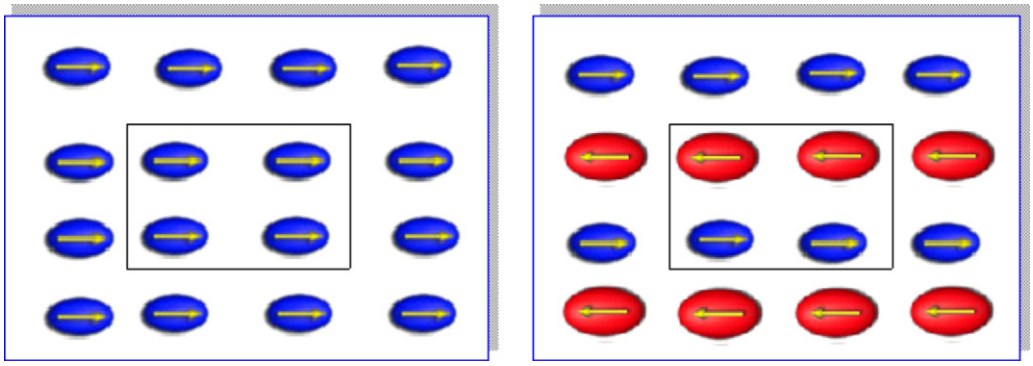

Fig. 4. Orientation of dipole moments.

angles are slightly higher than that of XRD values. These deviations can be attributed to the fact that the theoretical calculations were aimed at the isolated molecule in the gaseous phase whereas the XRD results were aimed at the molecule in the solid state.

3.2. Second harmonic generation (SHG) studies of dfppip

Second harmonic signal of 50 mV was obtained for dfppip by an input energy of 4.1 mJ/pulse. But the standard KDP crystal gave a SHG signal of 110 mV/pulse for the same input energy. The second order non-linear efficiency will vary with the particle size of the powder sample [25]. Higher efficiencies are achieved by optimizing the phase matching [26]. On a molecular scale, the extent of charge transfer (CT) across the NLO chromophore determines the level of SHG output, the greater the CT and the larger the SHG output.

3.3. Comparison of $\mu\beta_0$

The overall polarity of the synthesized imidazole derivative was small when their dipole moments were aligned in a parallel fashion (Fig. 4). When the electric field is removed, the parallel alignment of the molecular dipole moments begins to deteriorate and eventually the imidazole derivative loses its NLO activity. The ultimate goal in the design of polar materials is to prepare compounds which have their molecular dipole moments aligned in the same direction [27].

Theoretical investigation plays an important role in understanding the structure-property relationship, which is able to assist in designing novel NLO chormophores. The electrostatic first hyperpolarizability (β) and dipole moment (μ) of the imidazole chromophore have been calculated by using Gaussian 03 package [12]. From Table 3, it is found that the imidazole chromophore show larger $\mu\beta_0$ values, which is attributed to the positive contribution of their conjugation. This chromophore exhibits larger non-linearity and its λ_{max} is red-shifted when compared with unsubstituted imidazole. Therefore, it is clear that the hyperpolarizability is a strong function of the absorption maximum. Since even a small absorption at the operating wavelength of optic devices can be detrimental, it is important to make NLO chromophores as transparent as possible without compromising the molecule's nonlinearity. Thermal stability of the imidazole chromophore was estimated by thermo gravimetric analysis (TGA).

To determine the transference region and hence to know the suitability of dfppip for microscopic non-linear optical applications, the UV–visible spectra have been recorded by using the spectrometer in the range of 200–750 nm. The absorption spectrum of dfppip was shown in the UV region between 270 and 320 nm. The increased transparency in the visible region might enable the microscopic NLO behavior with non-zero values [28,29,14]. All the absorption bands are due to $\pi \rightarrow \pi^*$ transitions. The β values (Table 3) computed here might be correlated with UV–visible spectroscopic data in order to understand the molecular-structure

Table 3
Electric dipole moment (D), polarizability (α) and hyperpolarizability (β_{total}) of dfppip.

Parameter	(1)
Dipole moment (D)	
μ_x	−4.8837
μ_y	3.8654
μ_z	−1.1755
μ_{total}	6.3383
Polarizability (α)	
α_{xx}	−195.8733
α_{xy}	9.3770
α_{yy}	−151.0243
α_{xz}	−1.6154
α_{yz}	1.2928
α_{zz}	−167.2760
$\alpha \times 10^{-24}$ (esu)	−25.4002
Hyperpolarizability	
β_{xxx}	139.4198
β_{xxy}	4.8411
β_{xyy}	−26.7741
β_{yyy}	25.1737
β_{xxz}	10.8520
β_{xyz}	−1.5723
β_{yyz}	5.6214
β_{xzz}	59.6695
β_{yzz}	5.8253
β_{zzz}	−1.0489
$\beta \times 10^{-33}$ (esu)	54.7580
$\mu\beta \times 10^{-31}$ (esu)	347.0726

and NLO relationship in view of a future optimization of the microscopic NLO properties. The band at around 320 nm exhibits a solvatochromic shift, characteristic of a large dipole moment and frequently suggestive of a large hyperpolarizability. This compound show red shift in absorption with increasing solvent polarity, accompanied with the upward shifts non-zero values in the β-components.

3.4. Octupolar and dipolar components of dfppip

The imidazole derivative (dfppip) possess a more appropriate ratio of off-diagonal versus diagonal β tensorial component ($r = \beta_{xyy}/\beta_{xxx}$) which reflects the inplane non-linearity anisotropy and the largest $\mu\beta_0$ values. The difference of the β_{xyy}/β_{xxx} ratios can be well understood by analyzing their relative molecular orbital properties. The electrostatic first hyperpolarizabilities (β_0) and dipole moment (μ) of the chromophores have been investigated theoretically. These observed results can be explained by the reduced planarity in such chromophores caused by the steric interaction between the two phenyl rings at C(23) and N(15) atoms. Hence, the steric interaction must be reduced in order to obtain larger β_0 values.

The β tensor [30] can be decomposed in a sum of dipolar ($^{2D}_{J=1}\beta$) and octupolar ($^{2D}_{J=3}\beta$) tensorial components, and the ratio of these two components strongly depends on their 'r' ratios. The zone for $r > r_2$ and $r < r_1$ corresponds to a molecule of octupolar and dipolar, respectively. The critical values for r_1 and r_2 are $(1-\sqrt{3})/\sqrt{3}\sqrt{3}+1) = -0.16$ and $(\sqrt{3}+1)/\sqrt{3}(\sqrt{3}-1) = 2.15$, respectively. Complying with the Pythagorean theory and the projection closure condition, the octupolar and dipolar components of the β tensor can be described as:

$$\left\|^{2D}_{J=1}\beta\right\| = \left(\frac{3}{4}\right)\left[(\beta_{xxx}+\beta_{yyy})^2 + (\beta_{yyy}+\beta_{yxx})^2\right] \quad (6)$$

$$\left\|^{2D}_{J=3}\beta\right\| = \left(\frac{1}{4}\right)\left[(\beta_{xxx-3}\beta_{xyy})^2 + (\beta_{yyy-}\beta_{yxx})^2\right] \quad (7)$$

The parameter $\rho^{2D}[\rho^{2D} = \left\|^{2D}_{J=3}\beta\right\| / \left\|^{2D}_{J=1}\beta\right\|]$ is convenient to compare the relative magnitudes of the octupolar and dipolar components of β. The observed positive small ρ^{2D} value (0.096) reveals that the β_{iii} component cannot be zero and these are dipolar component. Since most of the practical applications for second order NLO chromophores are based on their dipolar components, this strategy is more appropriate for designing highly efficient NLO chromophores.

3.5. Natural bond orbital (NBO) analysis

NBO analysis have been performed for dfppip at the DFT/B3LYP/6-31++G(d,p) level in order to elucidate the intramolecular, hybridization and delocalization of electron density within the molecule. The importance of hyperconjugative interaction and electron density transfer (EDT) from lone pair electrons to the antibonding orbital has been analyzed and the results [31] were tabulated in Tables 4 and 5. Several donor–acceptor interactions

Table 4
Significant donor–acceptor interactions of dfppip and their second-order perturbation energies (kcal/mol).

Donor (i)	Type	ED/e	Acceptor (j)	Type	ED/e	$E(2)$ a.u.	$E(j)-E(i)$	$F(i,j)$
C1–C2	π	1.7096	C5–N14	π^*	0.0102	45.99	0.48	0.134
C3–C4	π	1.9720	C5–N14	π^*	0.0131	31.79	0.46	0.111
C5–N14	π	1.9879	C1–C2	π^*	0.0103	26.46	0.53	0.106
C5–C14	π	1.9879	C3–C4	π^*	0.0305	43.04	0.52	0.138
C6–C9	π	1.9713	N16–C23	π^*	0.0167	31.13	0.47	0.109
C7–C8	π	1.9735	C12–N13	π^*	0.0101	32.58	0.46	0.112
C10–C11	π	1.9814	C12–N13	π^*	0.0101	46.60	0.48	0.134
C12–N13	π	1.9878	C7–C8	π^*	0.0296	40.47	0.53	0.135
C12–N13	π	1.9878	C10–C11	π^*	0.0126	25.63	0.54	0.105
N16–C23	π	1.9824	C6–C9	π^*	0.0249	35.07	0.56	0.134
Lp N15	π	1.6487	C6–C9	π^*	0.0249	52.72	0.53	0.149
Lp N15	π	1.6487	N16–C23	π^*	0.0167	72.94	0.51	0.174
Lp F30	π	1.9414	C27–C29	π^*	0.0220	27.96	0.77	0.142
Lp F31	π	1.9414	C24–C25	π^*	0.0352	27.89	0.78	0.143
C3–C4	π	1.9720	C1–C2	π^*	0.0131	305.20	0.02	0.114
C3–C4	π	1.9720	C7–C8	π^*	0.0296	348.68	0.02	0.105
C5–N14	π	1.9879	C1–C2	π^*	0.0132	468.41	0.01	0.121
C6–C9	π	1.9713	C7–C8	π^*	0.0296	461.61	0.01	0.105
C7–C8	π	1.9735	C10–C11	π^*	0.0125	340.11	0.02	0.115
C12–N13	π	1.9878	C10–C11	π^*	0.0125	271.22	0.02	0.119
N16–C23	π	1.9824	C6–C9	π^*	0.0249	190.85	0.02	0.091
C17–C18	π	1.9760	C19–C21	π^*	0.0132	507.95	0.01	0.121
C17–C18	π	1.9760	C20–C22	π^*	0.0147	417.92	0.02	0.125
C24–C25	π	1.9760	C26–C28	π^*	0.0119	348.82	0.02	0.123
C27–C29	π	1.9813	C26–C28	π^*	0.0119	253.24	0.02	0.120

Table 5
Percentage of s and p-character on each natural atomic hybrid of the natural bond orbital.

Bond (A–B)	E_D/Energy (a.u.)	ED_A%	ED_B%	s%	p%
C4–N14	0.6459	41.71	58.26	30.20	69.80
	0.7635	–	–	35.64	64.36
C5–N14	0.6341	40.21	59.79	30.99	69.01
	0.7732	–	–	36.98	63.02
C6–N15	0.6064	36.78	63.22	27.33	72.67
	0.7951	–	–	33.10	66.9
C7–N13	0.6464	41.79	58.21	30.26	69.74
	0.7630	–	–	35.54	64.46
C9–N16	0.6464	41.79	58.21	28.98	71.02
	0.7630	–	–	32.99	67.01
C12–N13	0.6340	40.19	59.81	31.08	68.92
	0.7733	–	–	37.00	63.00
N15–C17	0.7966	63.46	36.54	35.02	64.98
	0.6045	–	–	26.67	73.33
N15–C23	0.8000	64.00	36.00	31.86	68.14
	0.6000	–	–	29.07	70.93
N16–C23	0.7634	58.28	41.72	35.36	64.64
	0.6459	–	–	32.91	67.09
C25–F31	0.5180	26.83	73.17	23.41	76.59
	0.8554	–	–	32.53	67.47
C29–F30	0.5181	26.85	73.15	23.60	76.40
	0.8553	–	–	32.53	67.47

are observed for the imidazole derivative (dfppip) and among the strongly occupied NBOs, the most important delocalization sites are in the π system and in the lone pairs (n) of the oxygen, fluorine and nitrogen atoms. The σ system shows some contribution to the delocalization, and the important contributions to the delocalization corresponds to the donor-acceptor interactions are C3–C4 → C1–C2, C3–C4 → C7–C8, C5–N14 → C1–C2, C6–C9 → C7–C8, C7–C8 → C10–C11, C12–N13 → C10–C11, N16–C23 → C6–C9, C17–C18 → C19–C21, C17–C18 → C20–C22, C24–C25 → C26–C28 and C27–C29 → C26–C28.

The charge distribution of dfppip was calculated from the atomic charges by NLO and NBO analysis (Fig. 5). These two methods predict the same trend i.e., among the nitrogen atoms N15 and N16, N15 is considered as more basic site [29]. The charge distribution shows that the more negative charge is concentrated on N15 atom whereas the partial positive charge resides at hydrogens. When compared to nitrogen atoms (N13, N14, N15 and N16),

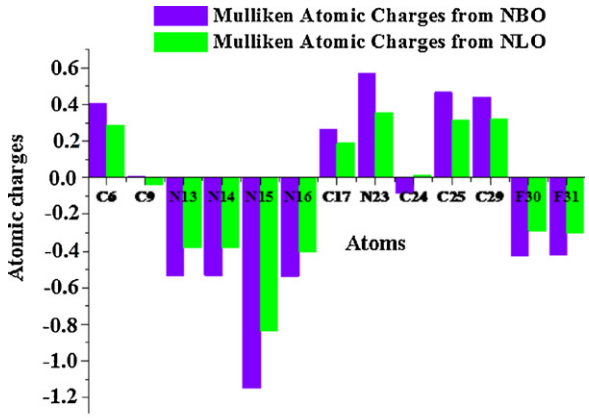

Fig. 5. Bar diagram representing the charge distribution of dfppip using NLO and NBO methods.

fluorine atoms (F30 and F31) are less electronegative in dfppip and among the nitrogen atoms N15 is considered as more basic site [32].

The percentage of s and p-character [33] in each NBO natural atomic hybrid orbital are displayed in Table 5. For all the carbon, nitrogen and fluorine atoms, around 60% of p-character and 30% s-character have been observed.

3.6. Molecular electrostatic potential map (MEP) and electronic properties

The molecular electrostatic potential surface MEP (Fig. 6) which is a plot of electrostatic potential mapped onto the iso-electron density surface simultaneously displays molecular shape, size and electrostatic potential values of the imidazole derivative (dfppip). MEP surface diagram is used to understand the reactive behavior of a molecule, in that negative regions can be regarded as nucleophilic centers, whereas the positive regions are potential electrophilic sites. The MEP map of dfppip clearly suggests that the nitrogen and fluorine atoms represent the most negative potential region. The hydrogen atoms bear the maximum brunt of positive charge. The predominance of green region in the MEP surfaces corresponds to

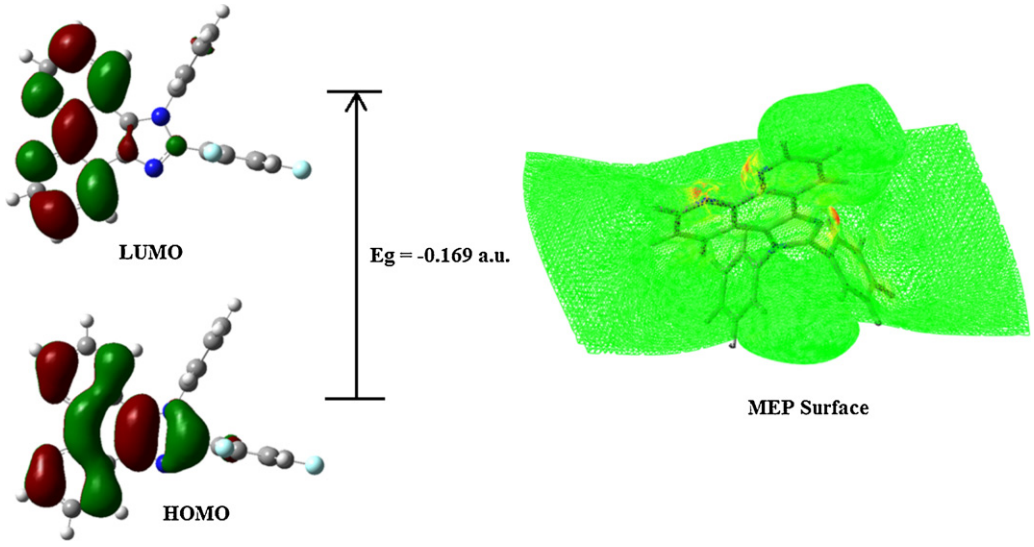

Fig. 6. HOMO–LUMO and MEP surface diagram of dfppip.

a potential halfway between the two extremes red and dark blue colour.

The HOMO is the orbital that primarily acts as an electron donor and the LUMO is the orbital that largely acts as the electron acceptor. The 3D plots of the frontier orbitals HOMO and LUMO of dfppip is shown in Fig. 6. The HOMO is located on the imidazole ring and phenanthroline ring, LUMO is located partly on the phenanthroline ring and C6, C9 and C24 atoms of the imidazole ring. The HOMO → LUMO transition implies that intramolecular charge transfer takes place [34] within the molecule. The energy gap (E_g) of dfppip has been calculated from the HOMO and LUMO levels. The decrease in the HOMO and LUMO energy gap explains the probable charge transfer (CD) taking place inside the chromophore.

4. Conclusion

We have reported a new, simple and an efficient route to the synthesis of biologically active heterocyclic substituted imidazole. The presence of α twist in this imidazole drops the fluorescence quantum yield. The observed dipole moment and hyperpolarizability can be explained by the reduced planarity caused by the steric interaction between the two phenyl rings at C(23) and N(15) atoms. Hence, the steric interaction must be reduced in order to obtain larger β_0 values. From the physicochemical studies, it was concluded that molecules of higher hyperpolarizability have larger dipole moments used as potential NLO molecules. The adjusted coefficient representing the acidity of the solvent, C_α or C_{SA} has a negative value, suggesting that the absorption and fluorescence bands shift to lower energies with the increasing acidity of the solvent.

Acknowledgments

One of the authors Dr. J. Jayabharathi, Associate professor, Department of Chemistry, Annamalai University is thankful to Department of Science and Technology [No. SR/S1/IC-07/2007] and University Grants commission (F. No. 36-21/2008 (SR)) for providing funds to this research study.

References

[1] J. Santos, E.A. Mintz, O. Zehnder, C. Bosshard, X.R. Bu, P. Gunter, Tetrahedron Lett. 42 (2001) 805–808.
[2] T. Kamidate, T. Segawa, H. Watanabe, K. Yamaguchi, Anal. Sci. 5 (1989) 429–433.
[3] U. Ucucu, N.G. Karaburun, I. Isikdag, Il Farmaco 56 (2001) 285–290.
[4] K. Mahanalingam, M. Nethaji, P.K. Das, J. Mol. Struct. 378 (1996) 177–188.
[5] R. Koch, J.J. Finnerty, T. Bruhn, J. Phys. Org. Chem. 21 (2008) 954–962.
[6] G. Ye, W.P. Henry, C. Chen, A. Zhou, C.U. Pittman Jr., Tetrahedron Lett. 50 (2009) 2135–2139.
[7] D.M. Mitchell, P.J. Morgan, D.W. Pratt, J. Phys. Chem. A 112 (2008) 12597–12601.
[8] G. Fischer, W.D. Rudorf, E. Kleinpeter, Magn. Reson. Chem. 29 (1991) 204–206.
[9] E. Kleinpeter, A. Schulenburg, Tetrahedron Lett. 46 (2005) 5995–5997.
[10] E. Kleinpeter, A. Koch, B. Mikhova, B.A. Stamboliyska, T.M. Kolev, Tetrahedron Lett. 49 (2008) 1323–1327.
[11] S.R. Flom, P.F. Barbara, Chem. Phys. Lett. 94 (1983) 488–493.
[12] M.J. Frisch, G.W. Trucks, H.B. Schlegel, G.E. Scuseria, M.A. Robb, J.R. Cheeseman, J.A. Montgomery, T. Vreven Jr., K.N. Kudin, J.C. Burant, J.M. Millam, S.S. Iyengar, J. Tomasi, V. Barone, B. Mennucci, M. Cossi, G. Scalmani, N. Rega, G.A. Petersson, H. Nakatsuji, M. Hada, M. Ehara, K. Toyota, R. Fukuda, J. Hasegawa, M. Ishida, T. Nakajima, Y. Honda, O. Kitao, H. Nakai, M. Klene, X. Li, J.E. Knox, P. Hratchian, J.B. Cross, C. Adamo, J. Jaramillo, R. Gomperts, R.E. Stratmann, O. Yazyev, A.J. Austin, R. Cammi, C. Pomelli, J.W. Ochterski, P.Y. Ayala, K. Morokuma, G.A. Voth, P. Salvador, J.J. Dannenberg, V.G. Zakrzewski, S. Dapprich, A.D. Daniels, M.C. Strain, O. Farkas, D.K. Malick, A.D. Rabuck, K. Raghavachari, J.B. Foresman, J.V. Ortiz, Q. Cui, A.G. Baboul, S. Clifford, J. Cioslowski, B.B. Stefanov, G. Liu, A. Liashenko, P. Piskorz, I. Komaromi, R.L. Martin, D.J. Fox, T. Keith, M.A. Al-Laham, C.Y. Peng, A. Nanayakkara, M. Challacombe, P.M.W. Gill, B. Johnson, W. Chen, M.W. Wong, C. Gonzalez, J.A. Pople, Gaussian 03, Revision C.02, Gaussian, Inc., Wallingford, CT, 2004.
[13] M. Wagener, J. Sadowsky, J. Gasteiger, J. Am. Chem. Soc. 117 (1995) 7769–7775.
[14] Y. Yang, W.J. Zhang, X.M. Gao, Int. J. Quantum Chem. 106 (2006) 1199–1207.
[15] S. Rosepriya, A. Thiruvalluvar, J. Jayabharathi, M. Venkatesh Perumal, R.J. Butcher, J.P. Jasinski, J.A. Golen, Acta Cryst. E67 (2011) o989.
[16] J. Jayabharathi, V. Thanikachalam, M. Venkatesh Perumal, N. Srinivasan, Spectrochim. Acta A 79 (2011) 236–244.
[17] J. Jayabharathi, V. Thanikachalam, M. Venkatesh Perumal, K. Saravanan, J. Fluoresc. (2011) 0878–883, doi:10 1007/s10895-011.
[18] Y. Marcus, Chem. Soc. Rev. 22 (1993) 409–416.
[19] C. Reichardt, Chem. Rev. 94 (1994) 2319–2358.
[20] E. Lippert, in: J.B. Birks (Ed.), Organic Molecular Photophysics, vol. 2, Wiley-Interscience, Bristol, England, 1975, p. 1.
[21] K. Dimroth, C. Reichardt, Liebigs Ann. Chem. 727 (1969) 93–105.
[22] M.J. Kamlet, R.W. Taft, J. Am. Chem. Soc. 98 (1976) 377–383.
[23] J. Catalan, V. Lopez, P. Perez, J. Fluoresc. 6 (1996) 15–22.
[24] P. Gayathri, J. Jayabharathi, N. Srinivasan, A. Thiruvalluvar, R.J. Butcher, Acta Crystallogr. E66 (2010) o1703.
[25] Y. Porter, K.M. OK, N.S.P. Bhuvanesh, P.S. Halasyamani, Chem. Mater. 13 (2001) 1910–1915.
[26] M. Narayana Bhat, S.M. Dharmaprakash, J. Cryst. Growth 236 (2002) 376–380.
[27] D. Steiger, C. Ahlbrandt, R. Glaser, J. Phys. Chem. B 102 (1998) 4257–4260.
[28] V. Crasta, V. Ravindrachary, R.F. Bharantri, R. Gonsalves, J. Cryst. Growth 267 (2004) 129–133.
[29] P. Wang, P. Zhu, W. Wu, H. Kang, C. Ye, Phys. Chem. Chem. Phys. 1 (1999) 3519–3525.
[30] S.F. Tayyari, S. Laleh, Z.M. Tekyeh, M.Z. Tabrizi, Y.A. Wang, H. Rahemi, Mol. Struct. 827 (2007) 176–187.
[31] J. Marshal, Ind. J. Phys. 7213 (1988) 659–661.
[32] G. Wang, F. Lian, Z. Xie, G. Su, L. Wang, X. Jing, F. Wang, Synth. Met. 131 (2002) 1–5.
[33] M. Szafran, A. Komasa, E.B. Adamska, J. Mol. Struct. 827 (2007) 101–107.
[34] K. Fukui, T. Yonezawa, H. Shingu, J. Chem. Phys. 20 (1952) 722–725.